REPORT

QUANTUM ENTANGLEMENT

Probing Rényi entanglement entropy via randomized measurements

Tiff Brydges[1,2]*, Andreas Elben[1,2]*, Petar Jurcevic[1,2], Benoît Vermersch[1,2], Christine Maier[1,2], Ben P. Lanyon[1,2], Peter Zoller[1,2], Rainer Blatt[1,2], Christian F. Roos[1,2]†

Entanglement is a key feature of many-body quantum systems. Measuring the entropy of different partitions of a quantum system provides a way to probe its entanglement structure. Here, we present and experimentally demonstrate a protocol for measuring the second-order Rényi entropy based on statistical correlations between randomized measurements. Our experiments, carried out with a trapped-ion quantum simulator with partition sizes of up to 10 qubits, prove the overall coherent character of the system dynamics and reveal the growth of entanglement between its parts, in both the absence and presence of disorder. Our protocol represents a universal tool for probing and characterizing engineered quantum systems in the laboratory, which is applicable to arbitrary quantum states of up to several tens of qubits.

Engineered quantum systems that consist of tens of individually controllable interacting quantum particles are currently being developed using a number of different physical platforms, including atoms in optical arrays (*1*–*3*), ions in radio-frequency traps (*4*, *5*), and superconducting circuits (*6*–*9*). These systems offer the possibility of generating and probing complex quantum states and dynamics particle by particle and are finding application in the near term as quantum simulators and in the longer term as quantum computers. As these systems are developed, more and more sophisticated protocols are required to characterize them—i.e., to verify that they are performing as desired and to measure quantum phenomena of interest.

A key property to measure in engineered quantum systems is entanglement; for example, for quantum simulators and computers to provide an advantage over their classical analogs, they must generate large amounts of entanglement between their parts (*10*). Furthermore, entanglement provides signatures of a wide range of phenomena, including quantum criticality and topological phases (*11*) as well as thermalization dynamics (*12*) and many-body localization (*13*, *14*). In addition, entanglement underpins the working mechanism of widely used numerical methods based on tensor network states (*11*).

Entanglement can be probed by measuring entanglement entropies. In particular, consider the second-order Rényi entropy

$$S^{(2)}(\rho_A) = -\log_2 \mathrm{Tr}(\rho_A^2) \qquad (1)$$

with ρ_A as the reduced density matrix for a part A of the total system described by ρ. If the entropy of part A is greater than the entropy of the total system—i.e., $S^{(2)}(\rho_A) > S^{(2)}(\rho)$—bipartite entanglement exists between A and the rest of the system (*15*). Thus, measuring the entropy of the whole system and that of its subsystems provides information about the entanglement contained in the system. Additionally, a measurement of the entropy of the total state ρ provides a test of the overall purity of the system, as for pure quantum states $S^{(2)}(\rho) = 0$.

Recently, a protocol to directly measure the second-order Rényi entropy, $S^{(2)}$, has been demonstrated, requiring collective measurements to be made on two identical copies ρ of a quantum system (*16*–*19*). In (*18*), that protocol was used to study entanglement growth and thermalization in a six-site Bose-Hubbard system, realized with atoms in an optical lattice.

Here, we introduce and experimentally demonstrate a different protocol to measure the second-order Rényi entropy $S^{(2)}$, which is based on and extends the proposals in (*20*–*23*). Key strengths of the protocol are that it requires preparation of only a single copy of the quantum system at a time and can be implemented on any physical platform with single-particle readout and control. In contrast to recently developed, efficient tomographic methods (*24*, *25*) to characterize weakly entangled states, our approach imposes no a priori assumption on the structure of the quantum state. Instead, it provides direct access to properties of the density matrix that are invariant under local unitary transformations, such as $S^{(2)}$, without the need for prior tomographic reconstruction. $S^{(2)}$ can therefore be estimated with a significantly lower number of measurements than is necessary for quantum state tomography (see last paragraph). In our experiments, we used the protocol to measure the dynamical evolution of entanglement entropy of up to 10-qubit partitions of a trapped-ion quantum simulator.

The key insight of the protocol is that information about the second-order Rényi entropies of a system is contained in statistical correlations between the outcomes of measurements performed in random bases. Specifically, for a system of N qubits, the approach (*21*) is to apply a product of single-qubit unitaries $U = u_1 \otimes \ldots \otimes u_N$, where each unitary u_i is drawn independently from the circular unitary ensemble (CUE) (*26*), and then to measure the qubits in a fixed (logical) basis. For each U, repeated measurements are made to obtain statistics, and the entire process is repeated for many different randomly drawn instances of U. The second-order Rényi entropy, $S^{(2)}$, of the density matrix ρ_A for an arbitrary partition $A = \{i[1], \ldots, i[N_A]\}$ of $N_A \leq N$ qubits is then obtained from

$$S^{(2)}(\rho_A) = -\log_2 \bar{X}, \text{ with } X =$$

$$2^{N_A} \sum_{s_A, s'_A} (-2)^{-D[s_A, s'_A]} P(s_A) P(s'_A) \qquad (2)$$

In Eq. 2, the bar denotes the ensemble average of (cross-) correlations of excitation probabilities $P(s_A) = \langle s_A | U_A \rho_A U_A^\dagger | s_A \rangle$; s_A are the logical basis states of partition A, $U_A = U|_A$ is the restriction of U to A, $D[s_A, s'_A]$ is the Hamming distance between s_A and s'_A, and † represents the Hermitian conjugate. $\bar{X}$ is equal to the purity $\mathrm{Tr}(\rho_A^2)$ of the density matrix ρ_A. Equation 2 represents an explicit formula, proven in the supplementary text (*27*), to reconstruct the second-order Rényi entropy of the subsystem of interest directly from statistical correlations between randomized measurements. As a result, compared with the recursive scheme presented in (*21*), an exponential overhead in the classical postprocessing is avoided.

For the partition of a single qubit, $N_A = 1$, the Bloch sphere provides a simple graphical representation to clarify the relation between the purities and the distribution of excitation probabilities (Fig. 1A). For a pure state, $\mathrm{Tr}(\rho_A^2) = 1$, the quantum state can be represented as a unit Bloch vector on the sphere, with random rotations leading to a uniform distribution of probabilities covering the full range [0, 1]. For a mixed state, $\mathrm{Tr}(\rho_A^2) < 1$, the length of the Bloch vector is less than 1, and the probabilities take values in a reduced interval. Generalizing to the multiqubit scenario, the purities are directly inferred from the mean of the statistical distribution of a weighted sum of cross-correlations by using Eq. 2. Examples of cross-correlations that were measured for different partition sizes of the trapped-ion system are shown in Fig. 1B, together with the estimated purities.

Our experiments were implemented by using strings of up to 20 trapped $^{40}Ca^+$ ions, each of which encodes a qubit that can be individually manipulated by spatially focused, coherent laser pulses. When dressed with suitably tailored laser fields, the ions are subject to a quantum evolution that is equivalent to a model of spins interacting through a long-range XY model (*28*) in the

[1]Center for Quantum Physics and Institute for Experimental Physics, University of Innsbruck, Innsbruck, Austria.
[2]Institute for Quantum Optics and Quantum Information, Austrian Academy of Sciences, Innsbruck, Austria.
*These authors contributed equally to this work.
†Corresponding author. Email: christian.roos@uibk.ac.at

Corrected 9 April 2020. See full text.

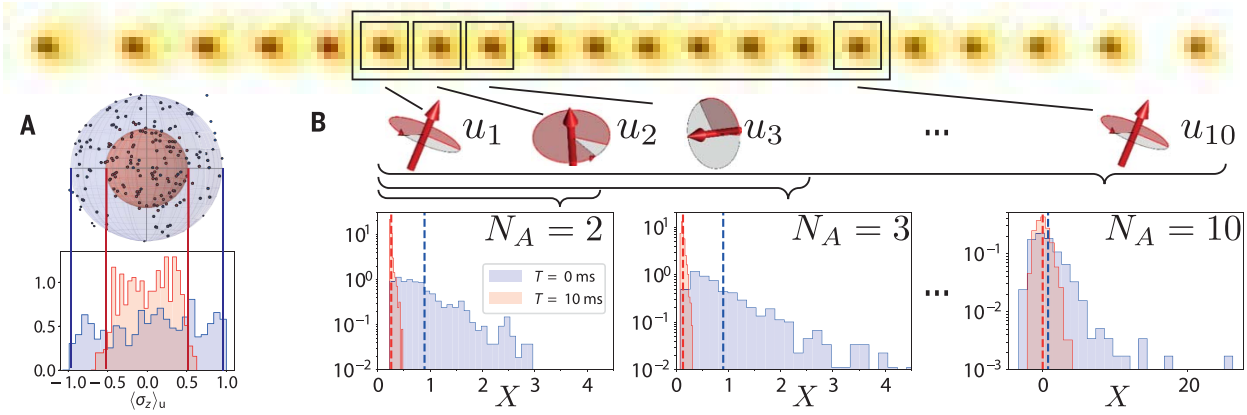

Fig. 1. Measuring second-order Rényi entropies through randomized measurements. (**A**) Single-qubit Bloch sphere. The purity is directly related to the width of the distribution of measurement outcomes after applying random rotations u_i. Initial pure state (blue) and mixed state (red) cases are shown. See text. (**B**) Generalization to multiple qubits: Measuring N_A-qubit (up to 10) partitions of a 20-qubit string, as shown (top). Repeated measurements (N_M = 150 and N_U = 500) were made to obtain statistics; see text. Experimental data (bottom): Histograms of the weighted sum X of cross-correlations (as defined in Eq. 2), with mean values corresponding to the purities (dashed lines). Results are shown for two different times during evolution under H_{XY} (Eq. 3), starting from a highly pure, separable state (blue) and evolving into a high-entropy state (red).

presence of a transverse field

$$H_{XY} = \hbar\sum_{i<j} J_{ij}(\sigma_i^+\sigma_j^- + \sigma_i^-\sigma_j^+) + \hbar B\sum_j \sigma_j^z \quad (3)$$

Here, $\hbar$ is Planck's constant divided by 2π, $\sigma_i^\beta(\beta = x, y, z)$ are the spin-½ Pauli operators, $\sigma_i^+(\sigma_i^-)$ the spin-raising (lowering) operators acting on spin i, and $J_{ij} \approx J_0/|i-j|^\alpha$ the coupling matrix with an approximate power-law decay and $0 < \alpha < 3$. For further experimental details, see (*27*, *29*). Optionally, a locally disordered potential could be added (*30*, *31*), realizing the Hamiltonian $H = H_{XY} + H_D$, with $H_D = \hbar\sum_j \Delta_j\sigma_j^z$ and Δ_j the magnitude of disorder applied to ion j. For entropy measurements, the following experimental protocol was used throughout: The system was initially prepared in the Néel ordered product state $\rho_0 = |\psi\rangle\langle\psi|$ with $|\psi\rangle = |\downarrow\uparrow\downarrow\ldots\uparrow\rangle$. This state was subsequently time-evolved under H_{XY} (or H) into the state $\rho(t)$. The coherent interactions arising from this time evolution generated varying types of entanglement in the system. Subsequently, randomized measurements on $\rho(t)$ were performed through individual rotations of each qubit by a random unitary (u_i), sampled from the CUE (*26*), followed by a state measurement in the z basis. Each u_i can be decomposed into three rotations $R_z(\theta_3)R_y(\theta_2)R_z(\theta_1)$, and two random unitaries were concatenated to ensure that drawing of the u_i was stable against small drifts of physical parameters controlling the rotation angles θ_i (*27*). Finally, spatially resolved fluorescence measurements realized a projective measurement in the logical z basis. To measure the entropy of a quantum state, N_U sets of single-qubit random unitaries, $U = u_1 \otimes \ldots \otimes u_N$, were applied. For each set of applied unitaries, U, the measurement was repeated N_M times.

In the first experiment, a 10-qubit state ρ_0 was prepared and subsequently time-evolved under H_{XY} (Eq. 3), without disorder, for $t = 0, \ldots, 5$ ms.

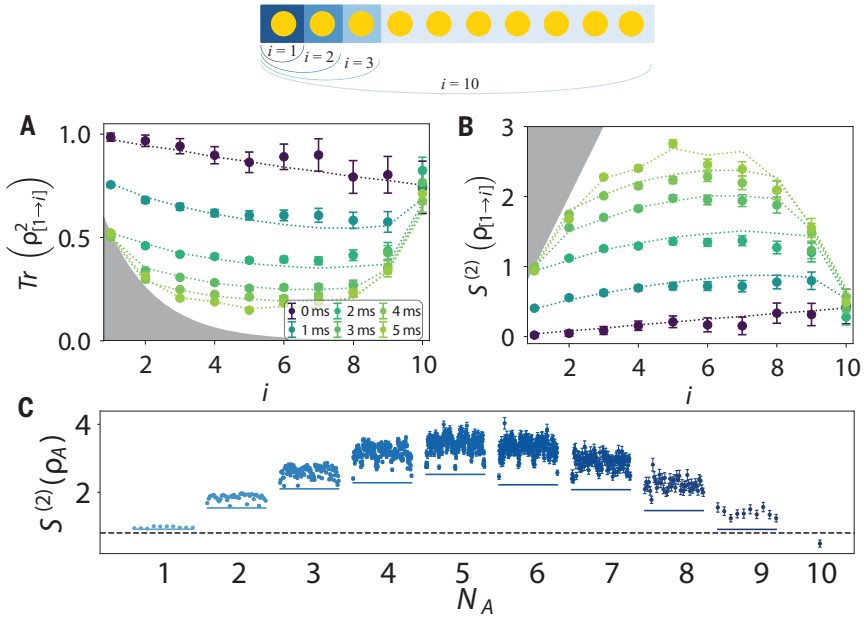

Fig. 2. Purity and second-order Rényi entropies of a 10-qubit system. (**A**) Measured purity and (**B**) second-order Rényi entropy of a Néel state, time-evolved under H_{XY} (J_0 = 420 s^{-1}, α = 1.24), for connected partitions $[1\to i]$. Dotted curves are purities derived from a numerical simulation; see supplementary materials (*27*). Maximally mixed states with minimal purity fall on the boundary of the shaded area. (**C**) Second-order Rényi entropy, $S^{(2)}(\rho_A)$, of all $2^{10} - 1 = 1023$ partitions at t = 5 ms, with N_A denoting the number of ions in a partition A. For all data points, N_M = 150 and N_U = 500. Error bars, which increase with subsystem size (*27*), are standard errors of the mean $\bar{X}$. Lines in (C) are drawn at three standard errors above the full system's entropy (black, dashed) and three standard errors below the minimal subsystem's entropy (blue, solid).

Figure 2, A and B, respectively show measured purities and entropies of all connected partitions that include qubit 1 during this quench. The overall purity (and thus entropy) remained at a constant value of $\mathrm{Tr}[\rho^2] = 0.74 \pm 0.07$, within error, throughout the time evolution, implying that the time evolution was approximately unitary. The initial state's reconstructed purity is in agreement with control experiments, which show a purity loss of 0.08 caused by imperfect state preparation and an underestimation of the purity by ~0.17 caused by decoherence during the random spin rotations (*27*). At short times, the single-spin subsystem became quickly entangled with the rest of the system, seen as a rapid decrease (increase) of the single-spin

Corrected 9 April 2020. See full text.

purity (entropy) (Fig. 2, A and B), until the reduced state became completely mixed. At longer times, the purity (entropy) of larger subsystems continued to decrease (increase), as they became entangled with the rest. The dotted curves represent numerical simulations for the experimental parameters, including decoherence, during state initialization, evolution, and measurement (*27*). Although Fig. 2, A and B, correspond to a specific set of connected partitions A, the data give access to the purities for all partitions A of the system, as shown in Fig. 2C for a specific time t = 5 ms. Because the second-order Rényi entropy of every subsystem is, within three standard deviations, larger than for the total system, this demonstrates entanglement between all $2^9 - 1 = 511$ bipartitions of the 10-qubit system.

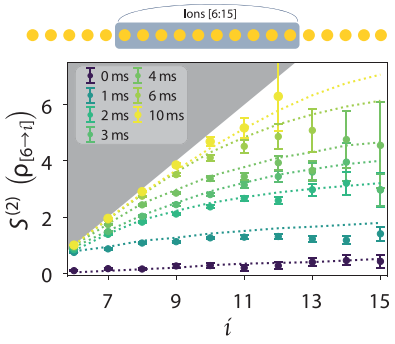

Fig. 3. Second-order Rényi entropy of 1- to 10-qubit partitions of a 20-qubit system. The initial low-entropy Néel state evolves under H_{XY} (J_0 = 370 s^{-1}, α = 1.01) within 10 ms into a state with high-entropy partitions, corresponding to nearly fully mixed subsystems. For the data taken at 6 ms (10 ms) of time evolution, the two (three) data points corresponding to highly mixed states are not shown, because they have large statistical error bars. For details regarding numerical simulations (dotted curves) and error bars, see (*27*).

Next, a 20-qubit experiment was performed, in which the entropy growth of the central part of the chain was measured during time evolution under H_{XY}, for partitions of up to 10 qubits. Our observations (Fig. 3) are consistent with the formation of highly entangled states. The entropy increases rapidly over the time evolution of 10 ms, with the reduced density matrices of up to seven qubits becoming nearly fully mixed. The experimental data agree very well with numerical simulations (dotted curves) obtained with a matrix-product state algorithm (*32*), which includes the (weak) effect of decoherence using quantum trajectories (*33*). The measurement highlights the ability of our protocol to access the entropy of highly mixed states, despite larger statistical errors compared with pure states (*27*).

Monitoring the entropy growth of arbitrary yet highly entangled states during their time evolution constitutes a universal tool for studying dynamical properties of quantum many-body systems, in connection with the concept of quantum thermalization (*12*). In this context, a slow entropy growth can be used to signify localization in generic many-body quantum systems (*14*). Generically, in interacting quantum systems without disorder, a ballistic (linear) entropy growth is predicted after a quantum quench (*12*). Such growth is assumed to persist until saturation is reached, signaling thermalization of the system at late times. On the contrary, in the presence of (strong) disorder and sufficiently short-ranged interactions, the existence of the many-body localized (MBL) phase (*13*) is predicted in one-dimensional systems (*34*). This phase is characterized by the absence of thermalization, the system's remembrance on the initial state (*35*) at late times, and, in particular, a logarithmic entropy growth (*36*, *37*), which constitutes the distinguishing feature between an MBL state and a noninteracting Anderson insulator. Experiments probing this entropy growth have been realized with superconducting qubits by using tomography (*8*) and ultracold atoms based on full-counting statistics of particle numbers (*38*). The persistence and stability of localization in long-range interacting systems have also been explored, both theoretically (*14*, *34*, *39*) and experimentally (*30*). The measurement of a long-time entropy growth rate is beyond the present capabilities of our trapped-ion quantum simulator, owing to its limited coherence time; however, we were able to observe the effects of local, random disorder on the entropy growth rate at early times.

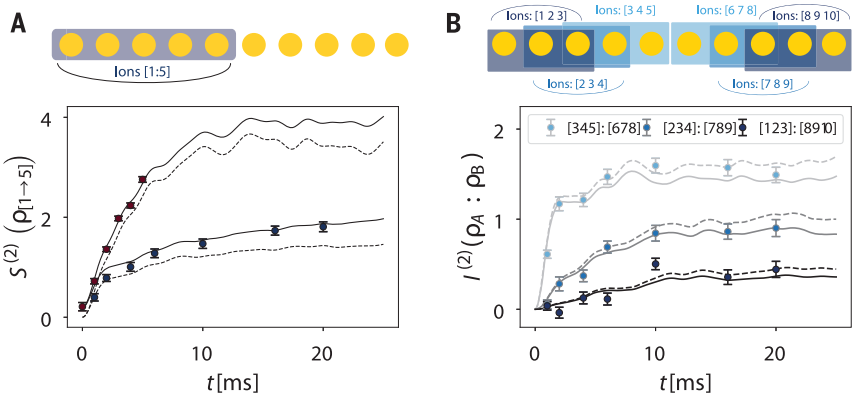

Fig. 4. Spread of quantum correlations under H_{XY} with and without disorder. The Hamiltonian parameters are J_0 = 420 s^{-1}, α = 1.24. (**A**) Half-chain entropy growth versus time without disorder (red data points) and with disorder, drawn uniformly from $[-3J_0, 3J_0]$ (blue data points). Numerical simulations based on unitary dynamics (dotted curves) including known sources of decoherence (full lines) are in agreement with the measured second-order Rényi entropies [see supplementary materials (*27*)]. (**B**) Second-order RMI of selected subsystems versus time in the presence of disorder (see Eq. 4). The decrease of $I^{(2)}$ with distance between subsystems is a manifestation of the inhibition of correlation spreading by local disorder. For longer time scales, decoherence leads to a slow increase in the entropy of the total system [$S^{(2)}(\rho) \approx 0.9$ for t = 10 ms for the full system (*27*)]. Consequently, there is an additional contribution to the slow entropy growth of the system from this decoherence, compared with the case of purely unitary dynamics. Error bars are the standard error of the mean, calculated with jackknife resampling of the applied random unitaries (*40*).

Figure 4A displays the measured evolution of the second-order Rényi entropy at half partition as a function of time, both in the absence and in the presence of local random disorder. Without disorder, a rapid, linear growth of entropy is observed, in agreement with theoretical simulations including the mentioned sources of decoherence (solid lines). To investigate the influence of disorder, the initial Néel state was quenched with $H = H_{XY} + H_D$, where the static, random disorder strength Δ_j was drawn uniformly from $[-3J_0, 3J_0]$. To efficiently access directly disorder-averaged quantities, our protocol offers the possibility to reduce the number of random unitaries that must be applied per disorder pattern and instead average in addition over different disorder patterns (*27*). Hence, only 10 random unitaries per disorder pattern (N_M = 150 measurements per unitary) and 35 randomly drawn disorder patterns were used to obtain an accurate estimate of the disorder-averaged purity $\overline{\mathrm{Tr}[\rho_A^2]}$ ($\overline{\ldots}$ denotes the disorder average) and subsequently the second-order Rényi entropy $\overline{S^{(2)}(\rho_A)} \approx -\log_2 \overline{\mathrm{Tr}[\rho_A^2]}$ (*27*). The measured, disorder-averaged entropy growth clearly demonstrates how disorder reduces the growth of entanglement. After an initial rapid evolution, a considerable slowing of the dynamics is observed, with a small but nonvanishing growth rate at later times, a behavior consistent with the scenario of MBL. The system retains memory of the initial Néel state during the dynamics, which is manifest in the measured time evolution of the local magnetization (fig. S5) (*27*).

Finally, Fig. 4B shows the evolution of the second-order Rényi mutual information (RMI), defined as

$$I^{(2)}(\rho_A : \rho_B) = S^{(2)}(\rho_A) + S^{(2)}(\rho_B) - S^{(2)}(\rho_{AB}) \quad (4)$$

In the presence of disorder, the RMI saturates quickly to approximately constant values, which decrease with increasing distance between the

Corrected 9 April 2020. See full text.

two partitions A and B. This indicates a spatial decay of correlations in the system, a characteristic feature of localization caused by the presence of disorder; this conclusion is supported by a numerical comparison of the RMI to the von Neumann mutual information, showing that they behave in qualitatively the same way (*27*).

In our experiments, we studied the entropy of partitions of up to 10 qubits because technical restrictions currently limit our experimental repetition rate. Straightforward technical improvements should allow the entropy of 20-qubit systems to be measurable. Numerical simulations (*27*) indicate that the total number of measurements required to access the purity within a statistical error of 0.12 is, for a pure product state of N_A qubits, given by $2^{7.7 \pm 0.3 + (0.8 \pm 0.1)N_A}$. The number of measurements required to obtain the purity of entangled pure states can be significantly lower (*27*). Purity measurements of systems containing tens of qubits are likely also in reach in experiments with high quantum state–generation rates, such as state-of-the-art superconducting qubit setups. The number of measurements could be further decreased by replacing the local random operations by global random unitaries acting on the entire Hilbert space of a subsystem of interest, by means of random quenches (*21*, *22*), at the expense of obtaining access to the purity of a single partition only.

REFERENCES AND NOTES

1. I. Bloch, J. Dalibard, S. Nascimbène, *Nat. Phys.* **8**, 267–276 (2012).
2. A. Browaeys, D. Barredo, T. Lahaye, *J. Phys. B* **49**, 152001 (2016).
3. M. Saffman, *J. Phys. B* **49**, 202001 (2016).
4. J. Zhang *et al*., *Nature* **551**, 601–604 (2017).
5. N. Friis *et al*., *Phys. Rev. X* **8**, 021012 (2018).
6. M. Fitzpatrick, N. M. Sundaresan, A. C. Y. Li, J. Koch, A. Houck, *Phys. Rev. X* **7**, 011016 (2017).
7. J. M. Gambetta, J. M. Chow, M. Steffen, *npj Quantum Inf.* **3**, 2 (2017).
8. K. Xu *et al*., *Phys. Rev. Lett.* **120**, 050507 (2018).
9. C. Neill *et al*., *Science* **360**, 195–199 (2018).
10. G. Vidal, *Phys. Rev. Lett.* **91**, 147902 (2003).
11. J. Eisert, M. Cramer, M. B. Plenio, *Rev. Mod. Phys.* **82**, 277–306 (2010).
12. P. Calabrese, J. Cardy, *J. Stat. Mech.* **2005**, P04010 (2005).
13. D. M. Basko, I. L. Aleiner, B. L. Altshuler, *Ann. Phys.* **321**, 1126–1205 (2006).
14. D. A. Abanin, E. Altman, I. Bloch, M. Serbyn, arXiv:1804.11065v1 [cond-mat.dis-nn] (30 April 2018).
15. R. Horodecki, P. Horodecki, M. Horodecki, K. Horodecki, *Rev. Mod. Phys.* **81**, 865–942 (2009).
16. A. K. Ekert *et al*., *Phys. Rev. Lett.* **88**, 217901 (2002).
17. R. Islam *et al*., *Nature* **528**, 77–83 (2015).
18. A. M. Kaufman *et al*., *Science* **353**, 794–800 (2016).
19. N. M. Linke *et al*., *Phys. Rev. A* **98**, 052334 (2018).
20. S. J. van Enk, C. W. J. Beenakker, *Phys. Rev. Lett.* **108**, 110503 (2012).
21. A. Elben, B. Vermersch, M. Dalmonte, J. I. Cirac, P. Zoller, *Phys. Rev. Lett.* **120**, 050406 (2018).
22. B. Vermersch, A. Elben, M. Dalmonte, J. I. Cirac, P. Zoller, *Phys. Rev. A* **97**, 023604 (2018).
23. A. Elben, B. Vermersch, C. F. Roos, P. Zoller, arXiv:1812.02624 [quant-ph] (6 Dec 2018).
24. B. P. Lanyon *et al*., *Nat. Phys.* **13**, 1158–1162 (2017).
25. G. Torlai *et al*., *Nat. Phys.* **14**, 447–450 (2018).
26. F. Mezzadri, *Not. Am. Math. Soc.* **54**, 592 (2007).
27. See supplementary materials.
28. D. Porras, J. I. Cirac, *Phys. Rev. Lett.* **92**, 207901 (2004).
29. P. Jurcevic *et al*., *Nature* **511**, 202–205 (2014).
30. J. Smith *et al*., *Nat. Phys.* **12**, 907–911 (2016).
31. C. Maier *et al*., *Phys. Rev. Lett.* **122**, 050501 (2019).
32. M. P. Zaletel, R. S. K. Mong, C. Karrasch, J. E. Moore, F. Pollmann, *Phys. Rev. B* **91**, 165112 (2015).
33. A. J. Daley, *Adv. Phys.* **63**, 77–149 (2014).
34. A. L. Burin, *Phys. Rev. B* **92**, 104428 (2015).
35. M. Schreiber *et al*., *Science* **349**, 842–845 (2015).
36. J. H. Bardarson, F. Pollmann, J. E. Moore, *Phys. Rev. Lett.* **109**, 017202 (2012).
37. M. Serbyn, Z. Papić, D. A. Abanin, *Phys. Rev. Lett.* **110**, 260601 (2013).
38. A. Lukin, M. Rispoli, R. Schittko, M. E. Tai, A. M. Kaufman, S. Choi, V. Khemani, J. Léonard, M. Greiner, arxiv:1805.09819 [cond-mat.quant-gas] (13 Jun 2018).
39. A. Safavi-Naini, M. L. Wall, O. L. Acevedo, A. M. Rey, R. M. Nandkishore, *Phys. Rev. A* **99**, 033610 (2019).
40. B. Efron, C. Stein, *Ann. Stat.* **9**, 586–596 (1981).
41. T. Brydges *et al*., Probing Rényi Entanglement Entropies via Randomized Measurements, Version 2, Zenodo (2018); https://doi.org/10.5281/zenodo.2527010.
42. T. Brydges *et al*., TiffBrydges/Renyi_Entanglement_Entropy v0, Zenodo (2019); https://doi.org/10.5281/zenodo.2533875.

ACKNOWLEDGMENTS

Funding: We acknowledge funding from the ERC Synergy Grant UQUAM, the European Research Council (ERC) under the European Union's Horizon 2020 research and innovation program under grant agreement no. 741541, the SFB FoQuS (FWF project no. F4016-N23), and QTFLAG–QuantERA. Also, the project leading to this application has received funding from the European Union's Horizon 2020 research and innovation programme under grant agreement no. 817482 (PASQUANS). **Author contributions:** P.Z. suggested the research topic, which was further developed by A.E., B.V., B.P.L., and C.F.R. A.E., B.V., and P.Z. developed the theoretical protocols. P.J., C.M., T.B., B.P.L., C.F.R., and R.B. contributed to the experimental setup. T.B., P.J., C.M., and C.F.R. performed the experiments. A.E., B.V., and C.F.R. analyzed the data and carried out numerical simulations. T.B., A.E., B.V., B.P.L., P.Z., and C.F.R. wrote the manuscript. All authors contributed to the discussion of the results and the manuscript. **Competing interests:** There are no competing interests. **Data and materials availability:** All data are publicly availableon Zenodo (*41*). All code used for data evaluation and numerical simulations is publicly available on Zenodo (*42*).

SUPPLEMENTARY MATERIALS

science.sciencemag.org/content/364/6437/260/suppl/DC1
Supplementary Text
Figs. S1 to S8
References (*43*–*46*)

15 June 2018; accepted 19 March 2019
10.1126/science.aau4963

Probing Rényi entanglement entropy via randomized measurements

Tiff Brydges, Andreas Elben, Petar Jurcevic, Benoît Vermersch, Christine Maier, Ben P. Lanyon, Peter Zoller, Rainer Blatt and Christian F. Roos

Science **364** (6437), 260-263.
DOI: 10.1126/science.aau4963

An entropic look into entanglement

Quantum systems are predicted to be better at information processing than their classical counterparts, and quantum entanglement is key to this superior performance. But how does one gauge the degree of entanglement in a system? Brydges *et al.* monitored the build-up of the so-called Rényi entropy in a chain of up to 10 trapped calcium ions, each of which encoded a qubit. As the system evolved, interactions caused entanglement between the chain and the rest of the system to grow, which was reflected in the growth of the Rényi entropy.

Science, this issue p. 260